



RESEARCH ARTICLE

10.1029/2021MS002561

On the Damping Time Scale of EVP Sea Ice Dynamics

 Sergey Danilov^{1,2,3} , Nikolay V. Koldunov¹ , Dmitry Sidorenko¹ , Patrick Scholz¹, and Qiang Wang¹ 
Key Points:

- Elastic Viscous Plastic (EVP) stability can be improved by proper selection of the time scale governing the decay of elastic waves
- A significant reduction of the required number of EVP sub-cycles can be achieved on high-resolution meshes
- EVP and the modified EVP simulate very similar sea-ice thickness and concentration

Correspondence to:
 S. Danilov,
sergey.danilov@awi.de
Citation:
 Danilov, S., Koldunov, N. V., Sidorenko, D., Scholz, P., & Wang, Q. (2021). On the damping time scale of EVP sea ice dynamics. *Journal of Advances in Modeling Earth Systems*, 13, e2021MS002561. <https://doi.org/10.1029/2021MS002561>

 Received 6 APR 2021
 Accepted 30 SEP 2021

¹Alfred Wegener Institute, Helmholtz Centre for Polar and Marine Research, Bremerhaven, Germany, ²Department of Mathematics and Logistics, Jacobs University, Bremen, Germany, ³A. M. Obukhov Institute of Atmospheric Physics RAS, Moscow, Russia

Abstract We propose to make the damping time scale, which governs the decay of pseudo-elastic waves in the Elastic Viscous Plastic (EVP) sea-ice solvers, independent of the external time step and large enough to warrant numerical stability for a moderate number of internal time steps. A necessary condition is that the forcing on sea ice varies slowly on the damping time scale, in which case an EVP solution may still approach a Viscous Plastic one, but on a time scale longer than a single external time step. In this case, the EVP method becomes very close to the recently proposed modified EVP (mEVP) method in terms of stability and simulated behavior. In a simple test case dealing with sea ice breaking under the forcing of a moving cyclone, the EVP method with an enlarged damping time scale can simulate linear kinematic features which are very similar to those from the traditional EVP implementation, although a much smaller number of internal time steps is used. There is more difference in sea-ice thickness and linear kinematic features simulated in a realistic Arctic configuration between using the traditional and our suggested choices of EVP damping time scales, but it is minor considering model uncertainties associated with choices of many other parameters in sea-ice models.

Plain Language Summary Numerical simulations of sea ice in ocean or climate models most frequently rely on the Elastic Viscous Plastic (EVP) method. Computational expenses of this method depend on its internal time step which is limited by the requirements of numerical stability. It is shown that some adjustment of dissipation time scale in the EVP method allows the time scale to be increased, thereby reducing the numerical costs without sacrificing the results of simulations.

1. Introduction

Most of the existing climate models rely on the Elastic Viscous Plastic (EVP) approach (Hunke & Dukowicz, 1997) to solve the sea-ice dynamics. The EVP solvers have been the subject of several recent papers which proposed a modification of the original EVP approach, called mEVP further (Bouillon et al., 2013; Kimmritz et al., 2015; Lemieux et al., 2012). In the mEVP approach, the aspects of convergence to the Viscous Plastic (VP) solution (Hibler, 1979) and numerical stability are separated, allowing stable performance independent of whether the solution is converged to the VP rheology. Despite the closeness between the EVP and mEVP there remains some vagueness on how they are related in terms of numerical stability and simulated dynamics. This note attempts to clarify some points by proposing a modified view on the EVP based on the stability argument, which puts the EVP and mEVP on an equal footing.

Our discussions in this note will be based on the stability analyses of Hunke and Dukowicz (1997) and Hunke (2001). The focus is not on the development of new sea-ice solvers, but rather on how to use traditional EVP in existing climate models to reach good numerical stability while keeping a high numerical efficiency. We will use 1D prototype equations to explain the stability issues. The conclusions from the stability analysis will be complemented by simulations performed with FESOM (Danilov et al., 2017), the sea-ice component of which is described in Danilov et al. (2015). The simulations are done on meshes with high horizontal resolution, which allow numerous linear kinematic features (LKFs) to be simulated with the EVP approach (see e.g., Wang et al., 2016). The EVP version used in FESOM is adjusted so that all the components of stresses tend to the VP stresses at the same rate. This improves stability (see, e.g., Bouillon et al., 2013; Danilov et al., 2015; Wang et al., 2016). Full equations solved with the EVP and mEVP methods can be found in papers cited above. A brief summary of their implementation in FESOM is given in the Appendices of Koldunov, Danilov, et al. (2019).

© 2021 The Authors. Journal of Advances in Modeling Earth Systems published by Wiley Periodicals LLC on behalf of American Geophysical Union. This is an open access article under the terms of the [Creative Commons Attribution-NonCommercial License](https://creativecommons.org/licenses/by-nc/4.0/), which permits use, distribution and reproduction in any medium, provided the original work is properly cited and is not used for commercial purposes.

2. The Stability of EVP

2.1. The Role of Pseudoelastic Time Scale T

Consider the following 1D prototype of the standard EVP equations (see, e.g., Hunke, 2001; Hunke & Dukowicz, 1997):

$$\partial_t \sigma = \frac{1}{2T} (\zeta \partial_x u - \sigma), \quad (1)$$

$$m \partial_t u = \partial_x \sigma + \tau, \quad (2)$$

where it is assumed that the motion is in the x -direction and depends on time and coordinate x ,

$$\zeta = \frac{P}{2 \max(\Delta, \Delta_{\min})},$$

u is the velocity, τ the wind and ocean forcing, and P the ice strength. Some numerical factors in these equations were discarded for simplicity (compare with Equation 20 in Hunke, 2001). The field Δ is the 1D version of

$$\Delta^2 = (\dot{\epsilon}_{11}^2 + \dot{\epsilon}_{22}^2)(1 + e^{-2}) + 4\dot{\epsilon}_{12}^2 e^{-2} + 2\dot{\epsilon}_{11}\dot{\epsilon}_{22}(1 - e^{-2}) \quad (3)$$

of the VP rheology, depending on the deformations in ice, where $e = 2$ and

$$\dot{\epsilon}_{ij} = \frac{1}{2} \left(\frac{\partial u_i}{\partial x_j} + \frac{\partial u_j}{\partial x_i} \right) \quad (4)$$

are the components of the strain rate tensor, with i, j being the x or y . We intend to make the equations tractable analytically, and assume the worst case in terms of stability when Δ is capped by its minimum value Δ_{\min} set to $2 \times 10^{-9} \text{ s}^{-1}$. We assume also that P is constant, leading to the constant viscosity ζ .

In the standard EVP, the time scale T is selected to be a fraction of the external time step Δt (see, e.g., Hunke, 2001). The Δt can be the time step of an ocean model if the sea ice is integrated together with the ocean, and we assume that this is the case. If $T/\Delta t$ is sufficiently small, then an equilibrium will be reached within the external time step Δt and the rhs of the σ -equation will approach zero, giving the VP regime

$$\sigma = \zeta \partial_x u.$$

Consider for a while the other balance in Equation 1:

$$\partial_t \sigma = \frac{1}{2T} \zeta \partial_x u,$$

which corresponds to “E” (elastic) in the EVP. Inserting it in the time differenced momentum (Equation 2) and neglecting forcing τ , we get

$$\partial_{tt} u = \partial_x \frac{P}{4Tm\Delta_{\min}} \partial_x u,$$

which is the wave equation with the phase speed

$$c^2 = \frac{P}{4Tm\Delta_{\min}}.$$

For $T = 10^3 \text{ s}$, $\Delta_{\min} = 2 \times 10^{-9} \text{ s}^{-1}$, $P = hP^*$ with $P^* = 3 \times 10^4 \text{ N/m}^2$ and $m = h\rho$ we get $c^2 \sim 4 \times 10^6 \text{ m}^2/\text{s}^2$ taking the ice density $\rho = 900 \text{ kg m}^{-3}$ (the mean thickness h drops out). The phase speed is rather large ($\approx 2,000 \text{ m/s}$), and limits the internal time step (substep) in the standard EVP as

$$c\Delta t_{EVP} = c\Delta t/N_{EVP} < C\Delta x, \quad (5)$$

leading to

$$N_{EVP} > c\Delta t/(C\Delta x), \quad (6)$$

where N_{EVP} is the number of substeps, C is a numerical factor on order one and Δx is the mesh cell size. For $\Delta x = 100 \text{ km}$ the time step limit is less than 50 s, which for $\Delta t = 1 \text{ hr}$ means $N_{EVP} > 70$.

However, when mesh is refined, the ratio of $\Delta t/\Delta x$ does not change much (if both Δt and Δx are set by the ocean model), while T becomes smaller if we keep the ratio of $T/\Delta t$ fixed. This increases c , implying an

increase in N_{EVP} as $(\Delta t)^{-1/2}$, thus a reduction in model numerical efficiency. Therefore, it is the desire to damp the pseudo-elastic waves within the external time step ($T/\Delta t < 1$) that causes the standard EVP to be more expensive on refined meshes.

As is known, we generally fail to damp these waves to the degree that a converged solution is reached (see, e.g., Koldunov, Danilov, et al., 2019). The decay of pseudo-elastic waves in the EVP is only exponential, roughly following $e^{-\Delta t/2T}$ per external time step in the 1D prototype here, so T should be unacceptably small for the solution to really approach the VP dynamics within the external time step Δt . The mEVP approach behaves similarly in this respect, with $e^{-N_{EVP}/\alpha}$ roughly defining the decay per time step, where α is the stability parameter.

To develop a heuristic argument let's take an oscillating forcing $\tau = \tau_0 e^{-i\omega t + ikx}$, where ω is the frequency of oscillations and k the wavenumber. In this case the solution $u = u_0 e^{-i\omega t + ikx}$ of Equations 1 and 2 is

$$u_0 = \frac{1 - 2i\omega T}{\omega(-i - 2\omega T)m + k^2 \zeta} \tau_0.$$

In order to approach the VP regime we need $2\omega T \ll 1$ in the numerator (the ζ term generally prevails in the denominator). If we have 3-hourly wind forcing, the largest frequency in forcing will be $\pi/3 \text{ h}^{-1}$, so $T \sim 1000 \text{ s}$ will correspond to $2\omega T \sim 0.6$. In reality, the local peak in high-frequency wind forcing is at the inertial frequency, which in high latitudes corresponds to $\pi/6 \text{ h}^{-1}$. Depending on the forcing used, the resolution (which might be too coarse to see the effects) and the compromise we are ready to make, T about 0.5 – 1 hr can be still sufficient to get solutions that are close to VP solutions. The selection of T becomes an experimental task.

If we fix T instead of varying it for different Δt , N_{EVP} needed for stability will be fixed too, losing the dependence on Δt and hence on the resolution if Δt and Δx are varying proportionally. The situation with EVP will then resemble the case with the split-explicit solvers for the sea surface elevation used in many ocean circulation models. They employ small internal time steps in order to be stable with respect to fast surface waves. The number of internal time steps is dictated by the wave phase speed, and generally does not depend on the mesh resolution because Δx and Δt are varied accordingly. For a fixed T and an appropriate value of N_{EVP} the EVP becomes similar to the mEVP proposed by Bouillon et al. (2013), as explained in the next section.

The total number of EVP internal steps per simulation depends on the internal time step governed by the speed of pseudo-elastic waves (see Equation 5). Therefore, even when sea-ice models are integrated with external time steps larger than in ocean models, the total number of internal time steps will not change and the overall efficiency of the EVP solver will not be increased.

2.2. EVP and mEVP

The pair of σ and u equations in EVP is integrated using forward-backward time stepping as

$$\begin{aligned} \sigma^{p+1} - \sigma^p &= \frac{\Delta t_{EVP}}{2T} (\zeta \partial_x u^p - \sigma^p), \\ m(u^{p+1} - u^p) &= \Delta t_{EVP} (\partial_x \sigma^{p+1} + \tau). \end{aligned}$$

Here p is the index of subcycling ($p = 0$ corresponds to the values at the end of external time step n , and the values at $p = N_{EVP}$ are those for $n + 1$).

The prototype form of mEVP is

$$\begin{aligned} \sigma^{p+1} - \sigma^p &= \frac{1}{\alpha} (\zeta \partial_x u^p - \sigma^p), \\ u^{p+1} - u^p &= \frac{1}{\beta} \left(u^n - u^p + \frac{\Delta t}{m} (\partial_x \sigma^{p+1} + \tau) \right). \end{aligned}$$

Here α and β are large parameters, and u^n is the velocity at the end of the last external time step. The iterative process can be considered as pseudo time stepping. We see that with $\alpha = 2T/\Delta t_{EVP}$ the σ -equations of EVP and mEVP become identical.

The u -equations are slightly different. The difference lies in the estimate of time derivative: it is time-local in EVP, but weighted between two estimates in mEVP. If we divide the u -equation of mEVP over

$\Delta t_{EVP} = \Delta t / N_{EVP}$ and then associate the time interval Δt_{EVP} with a single iteration of mEVP, $(u^{p+1} - u^p) / \Delta t_{EVP}$ is the time-local estimate of time derivative $\partial_t u$. The quantity $(u^p - u^n) / (p \Delta t_{EVP})$ is the mean time derivative $\overline{\partial_t u^p}$ over the time interval from n ($p = 0$) to p . The u -equation then becomes

$$m \left(\frac{\beta}{N_{EVP}} \partial_t u + \frac{p}{N_{EVP}} \overline{\partial_t u^p} \right) = \partial_x \sigma^{p+1} + \tau,$$

featuring an up-weighted time derivative, which leads to the response as if ice mass were larger than in reality (unless $\beta / N_{EVP} \ll 1$, which is seldom the case in practice). Accordingly, the transient response to fast changes in forcing will be slower. It is not the case for EVP, and in this respect the EVP is a more consistent option than mEVP unless $N_{EVP} \gg \beta$ in the latter.

We now compare stability conditions for both methods (see, e.g., Hunke, 2001, Equation 24, and Kimmritz et al., 2015, Equation 14). In the case of EVP, it is

$$N_{EVP}^2 > C_E \frac{\Delta t}{T} \frac{\zeta \Delta t}{m(\Delta x)^2}, \quad (7)$$

and in the case of mEVP method, it is

$$\alpha \beta > C_m \frac{\zeta \Delta t}{m(\Delta x)^2}. \quad (8)$$

Here C_E and C_m are numerical factors determined experimentally in realistic applications. $(\Delta x)^{-2}$ in both cases appears from an estimate of the maximum eigenvalue of $-\partial_{xx}$. It misses a numerical factor which depends on discretization and is hidden in C_E and C_m . We note that Equation 7 is the same as Equation 6, but written differently to facilitate a comparison with the mEVP case.

As mentioned, for EVP, if Δt and Δx vary proportionally on mesh refinement, stability does not depend on resolution for fixed T . For mEVP, the product $\alpha \beta$ needs to be increased with mesh refinement if $\Delta t \sim \Delta x$, as indicated by Equation 8.

Although mEVP does not pose explicit constraints on N_{EVP} , the need to approach to the VP solution implies that N_{EVP} should be related to α, β . If we write $\alpha = c_\alpha N_{EVP}$ and $\beta = c_\beta N_{EVP}$, with c_α and c_β the numerical factors, then the ratio $T / \Delta t$ in EVP plays the role of the product $c_\alpha c_\beta$ in mEVP as concerns stability (up to a numerical factor hidden in C_E and C_m). The stability is achieved by similar means in EVP and mEVP: to keep N_{EVP} moderate, one takes large $T / \Delta t$ in EVP or large $c_\alpha c_\beta$ in mEVP. For example, Koldunov, Danilov, et al. (2019) report mEVP simulations that were run with $\alpha = \beta = 500$ and $N_{EVP} = 100$, which should be similar to EVP case with $T / \Delta t = 25$, which corresponds to T about several hours.

In summary, in both cases using relatively low N_{EVP} affects the formal convergence to VP solutions. Whether or not such a choice of N_{EVP} is acceptable depends on the presence of high-frequency components in forcing, and can be evaluated through simulations for both EVP and mEVP (see, e.g., Kimmritz et al., 2017). On high-resolution meshes the results can be further affected by LKFs emerging in simulations, which remains to be seen.

The next two sections present results illustrating the consistency between the EVP and mEVP solutions in an idealized test case and in realistic simulations in the Arctic Ocean. Both cases develop multiple LKFs, and their pattern is used as one of criteria to judge on the consistency.

In practice, moderate violation of Equation 7 or 8 in, respectively, EVP or mEVP simulations does not imply numerical instability, but rather noise in strain rates. The noise distorts sea-ice dynamics and should be avoided. We therefore will continue to use the term “stability” in the sense of Equation 7 or 8.

3. Idealized Test Case

We run the test case described in Mehlmann et al. (2021) on a triangular mesh with the triangle side of 2 km. The sea ice occupies a rectangular box of 512 by 512 km in size. It is deformed by stresses due to a cyclone traveling along the diagonal toward the north-east corner. The initial ice concentration is 1, the initial thickness is approximately 0.3 m, with small modulation, $P^* = 3 \times 10^4 \text{ N/m}^2$, and $\Delta_{min} = 2 \times 10^{-9} \text{ s}^{-1}$. We compare the pattern of simulated LKFs at the end of the second day of simulations. The ice thickness is

Table 1
The Parameters of Runs Performed With Elastic Viscous Plastic (EVP) and Modified EVP

Run	Δt , min	T min	α, β	N_{EVP}
S1	2	60		100
S2	2	25		100
S3	2	0.25		1,000
M1	2		500	100
M2	2		500	3,000

relatively thin, and does not change substantially except for the northern and partly eastern boundaries. The simulated ice velocities in this test case allow the external time step Δt to be larger than 30 min if judged only by sea-ice advection. However, the external time step Δt is set to 2 min in all runs, which is a value expected from an ocean model running on a 2 km mesh in high latitudes.

Table 1 specifies the parameters of runs presented in Figures 1 and 2. We keep N_{EVP} low in S1, S2 and M1, and take T or α, β that ensure stability.

Figure 1 illustrates the behavior of EVP solutions with different parameters. Shown are the field of ice concentration and Δ . In S1, T is larger than needed for stability for the selected external time step Δt . S2 uses the lowest T that ensures stability. The difference between the results from S1 and S2 is very minor. If T is further reduced for N_{EVP} fixed (not shown),

noise starts to appear in Δ and velocity strain rates. It is localized in the corners, where the strain rates are small, down to $T = 15$ min. Although the solutions remain very close to S2 elsewhere (not shown), larger areas might be affected in longer simulations, and such T are not allowed. If T is increased further than in S1, some reduction in number of LKFs is generally noticeable (not shown). As mentioned above, the question on admissible T depends on temporal scales present in forcing and possibly on spatial resolution.

Run S3 has $T/\Delta t = 0.125$, to allow for a decay of pseudoelastic waves within the external time step, as intended in the traditional EVP. Note that the ratio is smaller than the commonly used value of 1/3 (Hunke, 2001) to ensure stronger decay. N_{EVP} is 10 times larger than in S1 and S2, which is dictated by stability condition (Equation 7) as the consequence of strong reduction in $T/\Delta t$. It can be seen that there are only very minor differences between the results of S3 and those of S1 and S2 in details. However, the EVP solver efficiency in S1 and S2 is 10 times higher than in S3. Simulation with $\Delta t = 30$ min, $T = 3$ min and $N_{EVP} = 4500$ carried out to reach small $T/\Delta t$ in a more economical way (not shown) results in patterns almost identical to S3, but are still about three times more expensive than S2.

Figure 2 compares the EVP and mEVP solutions. The parameters α, β and N_{EVP} in M1 imply that its $c_\alpha c_\beta \sim T/\Delta t$ of S1 and S2. While the details in the LKF pattern in S2 and M1 are not identical, the difference is minor. This leads us to conclude that EVP with the specified T behaves very similarly to mEVP, and there is no practical argument to prefer one over another. M2 keeps the same parameters as M1, except for 30 times larger N_{EVP} . Now N_{EVP} is much larger than α, β , which formally should lead to a closer convergence

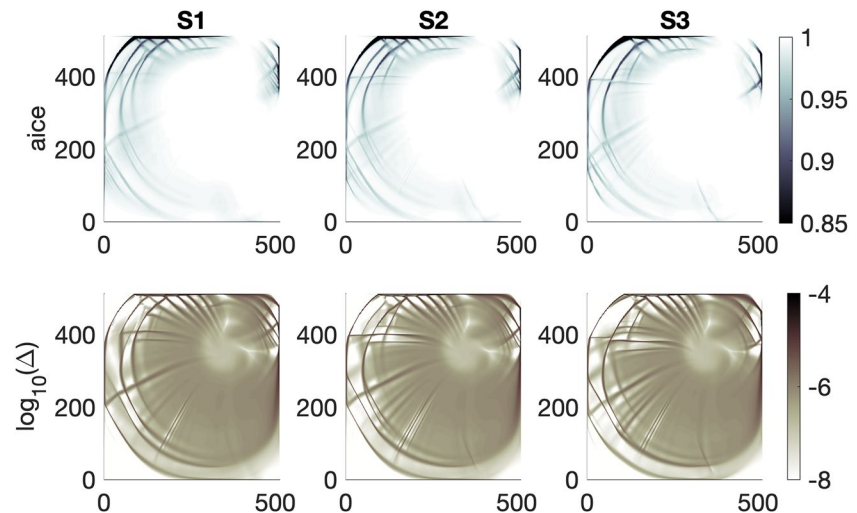


Figure 1. Ice concentration (top row) and Δ (bottom row) in test case runs with the Elastic Viscous Plastic method. S1 differs from S2 by larger T ($T = 1$ hr vs. $T = 1500$ s), which leads to minor differences in detail. S2 and S3 differ in the ratio $\Delta t/T$ by two orders of magnitude, but simulate close patterns.

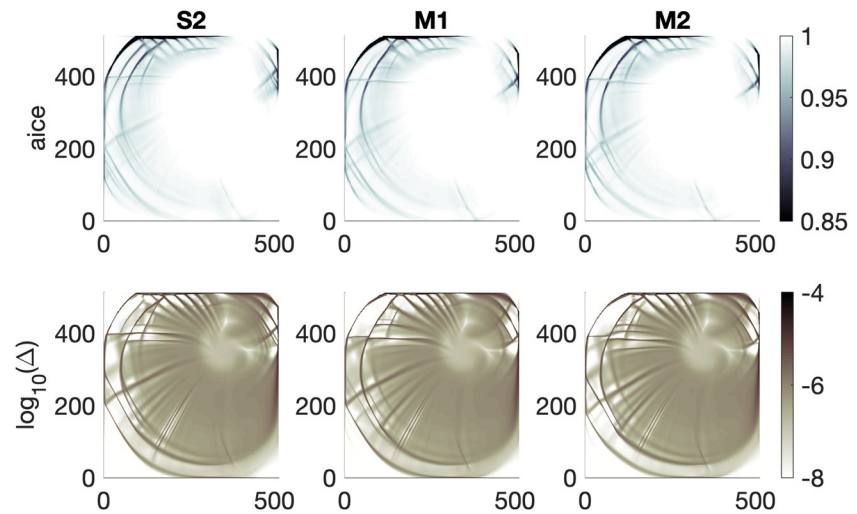


Figure 2. Ice concentration (top row) and Δ (bottom row) in test case runs with Elastic Viscous Plastic (EVP) and modified EVP solvers. S2 and M1 have the same $N_{EVP} = 100$. While there are small differences in details, the patterns of linear kinematic features agree between EVP and mEVP runs. M2 differs from M1 taking $N_{EVP} = 3000$ instead of 100. The increase in N_{EVP} causes little additional changes in model results when stability is ensured.

to the VP regime. Once again, this increase in N_{EVP} creates only minor differences, emphasizing the fact that in mEVP N_{EVP} is only required to be high enough to ensure some initial error reduction in the iterative process. As expected from the analysis above, increasing α, β for fixed N_{EVP} in mEVP will eventually lead to an effect similar to that of increasing T in EVP, filtering high-frequency response to forcing (not shown).

As concerns the differences between the simulated LKF patterns, we should note that the patterns depend, in addition to forcing and rheology, also on the details of numerical discretization. This is not surprising because LKFs are forming close to the grid scale, where all discretized differential operators contain numerical errors. As shown in Mehlmann et al. (2021), the change in the type of discretization, for example the placement of velocities on triangle centers or edges, induces much larger differences in the patterns of LKFs than those seen in Figures 1 and 2.

4. Arctic Simulations

Here our intention is to demonstrate that the EVP with fixed T also compares well with the standard EVP and mEVP in realistic model configurations. Simulations are carried out with FESOM2 in the global configuration used in Koldunov, Danilov, et al. (2019) where the Arctic Ocean is resolved at 4.5 km in terms of grid triangle height. We initialize the model in the year 1978 with PHC3 climatology (Steele et al., 2001) and 2 m ice where surface ocean temperature is below freezing point. The model is forced by JRA55-do reanalysis fields (Tsujino, 2018), which have horizontal resolution of about 55 km and temporal interval of 3 hr. This setup gives an opportunity to observe development of sea-ice fields starting from a uniform sea-ice distribution, but under realistic forcing and for realistic geometry.

We performed six experiments. The EVP and mEVP experiments use $N_{EVP} = 100$ if not otherwise stated. Relying on the test case above and expression 7, we expect that $T \approx 2$ hr will lead to stable simulations in this case. The increase in T from 25 min in S2 is related to a 2.2 times higher ratio $\Delta t/\Delta x$ in Arctic simulations. The standard EVP run with $T = 2$ hr is labeled EVP2H, and the standard mEVP run with $\alpha = \beta = 500$ is labeled mEVP500. An additional EVP experiment is run with $T = 1$ hr (labeled EVP1H). An additional mEVP experiment is run with $\alpha = \beta = 800$ (labeled mEVP800). The other two experiments use the original EVP implementation (with $T = \Delta t/3$ as in Hunke, 2001) and differ in the value of N_{EVP} , with EVP0 having $N_{EVP} = 100$ and EVP0_600 having $N_{EVP} = 600$. EVP1H and EVP0 violate Equation 7, but to a different extent. EVP2H and EVP0_600 are close to the stability boundary, mEVP500 has a slightly stronger stability than EVP2H and EVP0_600, and mEVP800 is even more stable. For convenience, the parameters are listed in Table 2. Since EVP0_600 uses the standard selection of T , it provides a baseline for comparison. The daily

Table 2
The Parameters of Arctic Ocean Runs Performed on a 4.5 km Mesh, and Resulting Model Run Time per Year of Simulations

Run	Δt , min	T min	α, β	N_{EVP}	1 year run time, min
EVP2H	10	120		100	75
mEVP500	10		500	100	75
EVP0_600	10	3.3		600	110
EVP1H	10	60		100	75
mEVP800	10		800	100	75
EVP0	10	3.3		100	75

Note. EVP, Elastic Viscous Plastic.

mean spatial distributions of Δ on October 27, 1980 (Figure 3) are quite similar for all experiments, except for EVP0. The large-scale spatial patterns of LKFs in Δ , defined by the forcing and ability of rheology to react to it, show good resemblance. The parameters in these simulations are selected such that the standard runs are not very far from their stability boundary. Run EVP1H, where the parameter T is lower than needed, reproduces a pattern of Δ that is very close to that of EVP2H. Daily averaging smooths small-scale noise, which is seen in instantaneous snapshots in EVP1H (not shown). Although run EVP2H is similar to S2 in terms of stability, it was found to sporadically develop some noise in the field of Δ . This means that T in EVP2H should be slightly increased for optimal performance.

In run mEVP800 the parameters α, β are excessively high. Some differences between mEVP500 and mEVP800 can be seen in some of the long LKFs and in the position and numbers of LKFs near ice edges. However, the differences are rather minor. Although we do not illustrate it, the

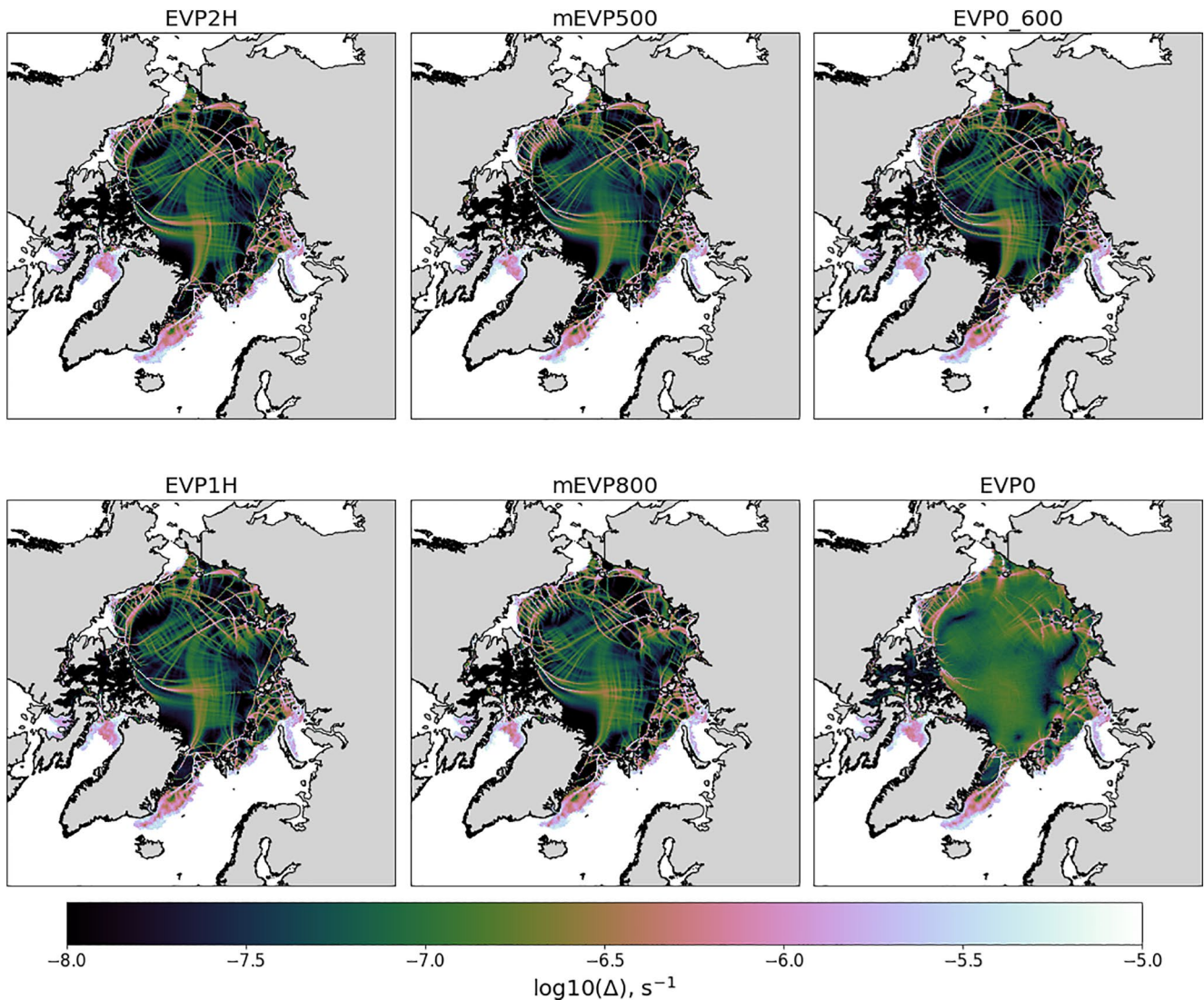


Figure 3. Spatial distribution of Δ fields at October 27, 1980 for simulations initialized at January 1 with 2 m thick ice, 1978 and run with JRA55-do forcing.

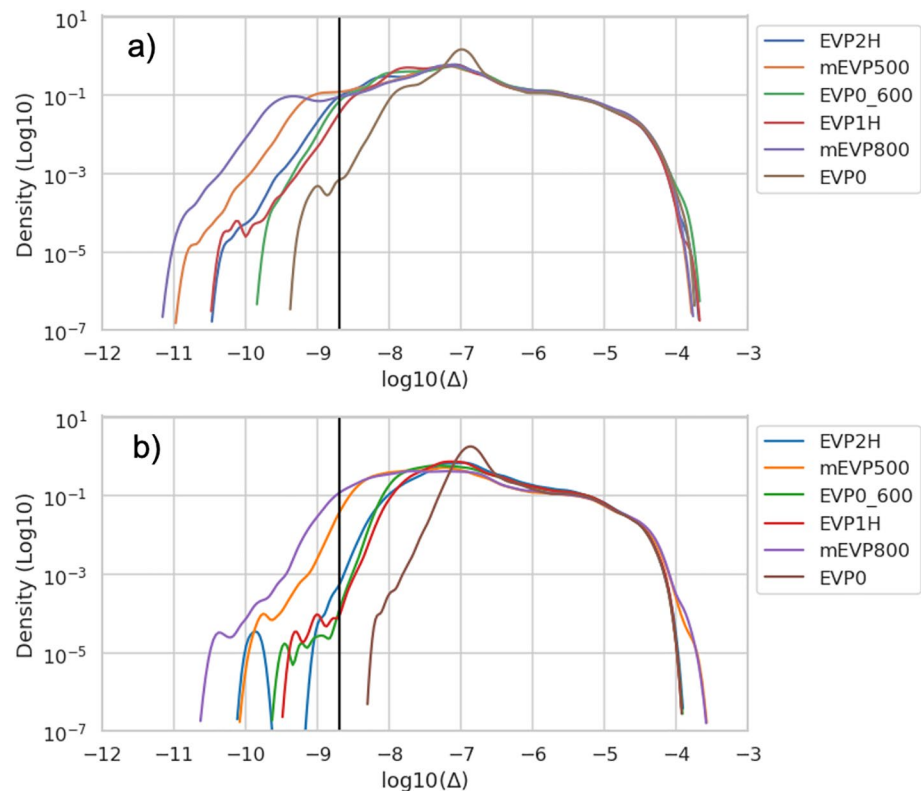


Figure 4. The probability density function (PDF) of Δ [1/s] on October 27, 1980 based on daily mean (top) and instantaneous (bottom) fields. The vertical line corresponds to $\Delta = \Delta_{min} = 2 \times 10^{-9} \text{ s}^{-1}$.

results from EVP and mEVP runs remain very similar when T (in case of EVP solver) and α, β (in case of mEVP solver) are increased in some limits beyond the values listed in Table 2.

The comparison of EVP0 and EVP0_600 (Figure 3, right column) shows that the picture of deformations using the original EVP implementation becomes close to those of mEVP and EVP with adjusted T only if N_{EVP} is significantly increased to ensure Equation 7. This, however, increases the computational cost of the sea-ice model in our setup from about 20% of the ocean model in case of $N_{EVP} = 100$ to about 100% in the case of $N_{EVP} = 600$ (see also Figure 1 in Koldunov, Danilov, et al., 2019). The situation may become worse with an increase in the number of computational cores. Although the EVP method scales well when the number of cores is increasing, it saturates earlier than the ocean model because it needs inter-core communications after each subcycle (Koldunov, Aizinger, et al., 2019). Simply increasing T to an appropriate higher value allows the computational cost of the EVP solver to be kept the same low as for the mEVP solver ($N_{EVP} = 100$). The overly smooth pattern of Δ seen in EVP0 is related to noise smoothed by daily averaging. It leads to distorted distribution of internal stresses and different dynamics.

For a more quantitative analysis, the top panel of Figure 4 presents the probability density functions (PDF) for the daily mean patterns of Figure 3. The PDF is similar for $\Delta > 5 \times 10^{-8} \text{ s}^{-1}$ for all runs except EVP0. EVP and mEVP runs are grouping together (again, with exception of EVP0), but they are more distinct for snapshots (bottom panel). Interestingly, EVP1H and EVP2H differ not very substantially in the Δ PDF despite EVP1H being slightly unstable.

While the patterns of Δ in Figure 3 are rather close for all runs except EVP0, small differences in sea-ice dynamics and, hence, thermodynamics accumulate with time, and may result in noticeable differences in sea-ice thickness regionally. The sea-ice thickness snapshot at October 27, 1980 (Figure 5) shows that the general spatial pattern of the sea-ice thickness is similar between the EVP and mEVP runs that respect numerical stability requirements. Sea ice thickness distribution the most similar to that in EVP0_600 is obtained in the run mEVP500. The sea ice simulated in EVP2H is slightly thinner, indicating that some increase in T above

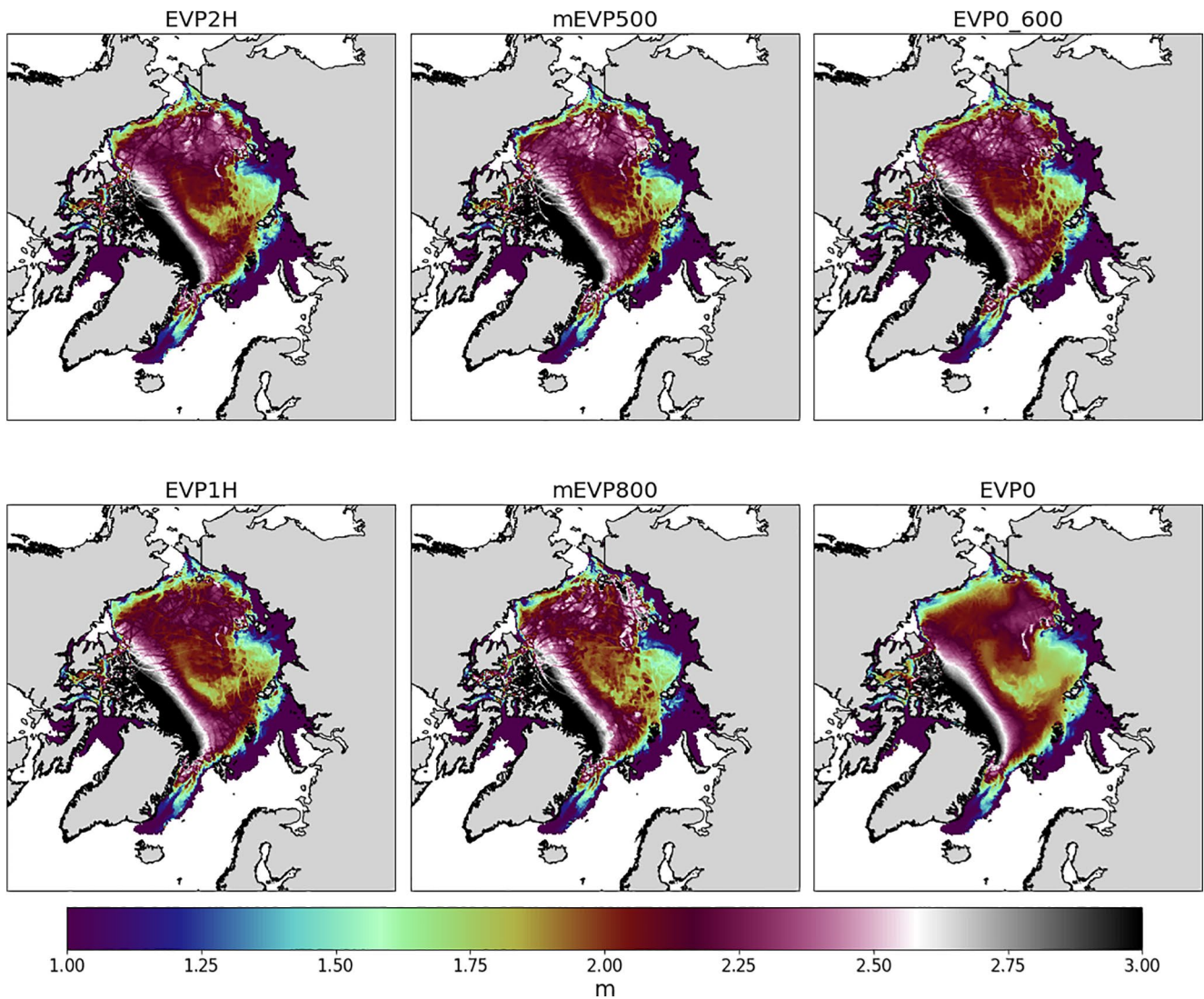


Figure 5. Spatial distribution of sea-ice thickness at October 27, 1980 for simulations with different EVP versions and settings (summarized in Table 2).

2 hr is still needed in this case, as already mentioned. Runs EVP0 and EVP1H are obvious outliers, showing a reduced thickness. We refrain from quantifying the differences in the number of LKFs and describing effects on the behavior of the sea ice and ocean properties, which is reserved for future dedicated studies.

5. Discussions

To make the cost of the EVP sea-ice solver moderate, we selected N_{EVP} around 100 and determined the time scale T (around 1–2 hr) that ensures numerical stability. The numbers given here can be used as guiding, but in each case the final choice is experimental. For given forcing and resolution, there generally exist a range of T where the differences between simulations are relatively small with respect to the well behaving case (EVP0_600 here). If such a range is identified, there is also some freedom in selecting the number of internal steps N_{EVP} : it can be even further reduced without violating stability if higher values of T are taken (according to Equation 7, doubling T allows a factor of $\sqrt{2}$ decrease in N_{EVP}). However, an increase in T beyond some bound will have implications for sea-ice dynamics as discussed above.

If T needed for stability appears to be too large (e.g., for some high-resolution forcing), N_{EVP} has to be increased to maintain stability for an appropriate T . For example, in Arctic simulations above, $N_{EVP} = 200$ would allow T smaller than 1 hr.

The mEVP approach masks these issues because its numerical stability does not depend on N_{EVP} . However, high ratios of α, β to N_{EVP} needed to ensure stability and low computational cost, are similar to $\Delta t/T$ ratio in EVP and imply possible divergence from the VP regime.

Similar to the adaptive approach proposed for the mEVP solver in Kimmritz et al. (2016), the selection of T in EVP can also be done adaptively. Indeed, high values of T are only necessary in certain areas where ice strain rates are low and viscosities of the VP rheology are high. The values of T necessary for stability at a particular location can be diagnosed at the end of external time steps based on Equation 7 with experimentally determined C , and used locally at each grid cell over the next external step. We did not try this in FESOM yet.

6. Conclusions

The elementary analysis and examples above can be summarized as follows.

1. EVP becomes very similar to mEVP in terms of stability if T of EVP is taken constant and sufficiently large (about 1–2 hr) and if adjustments are made to ensure the same decay for all components of stress tensor. N_{EVP} can then be kept relatively low (about 100) independent of resolution, provided that Δt is varied proportionally to Δx . mEVP will still require some adjustment of α, β to mesh refinement if Δt is varied proportionally to Δx .
2. This leads to a conceptual change: the background pseudoelastic waves in solutions are admitted, whereby the EVP solution becomes slightly different from the VP solution. These waves are slowed down through the choice of T in EVP or α, β in mEVP for stability with affordable N_{EVP} .
3. The reaction of ice to fast varying forcing is likely to be affected in both EVP and mEVP if T or α, β are high. Both cases are a compromise between the computational demand (moderate N_{EVP}) and closeness to VP solutions. However, the VP rheology is also an approximation.

We believe that our conclusions and illustrations are of practical interest and could guide the selection of sea-ice model parameters.

Acknowledgments

The authors are indebted to C. Rousset, E. C. Hunke, and an anonymous reviewer for valuable comments that helped to improve the presentation. The authors thank the developers of xarray (Hoyer & Hamman, 2017), numpy (Harris et al., 2020), cartopy (Met Office, 2010–2015), and matplotlib (Hunter, 2007) for making their code available on a free and open-source basis. This study is a contribution to the project S2: Improved parameterisations and numerics in climate models, S1: Diagnosis and Metrics in Climate Models and M5: Reducing spurious diapycnal mixing in ocean models of the Collaborative Research Centre TRR 181 “Energy Transfer in Atmosphere and Ocean” funded by the Deutsche Forschungsgemeinschaft (DFG, German Research Foundation)—project no. 274762653, and the Helmholtz initiative REKLIM (Regional Climate Change). This study has benefited from funding from the Initiative and Networking Fund of the Helmholtz Association through the project “Advanced Earth System Modelling Capacity (ESM)”. Open access funding enabled and organized by Projekt DEAL.

Data Availability Statement

The data and code to reproduce figures from this manuscript are available from Danilov et al. (2021).

References

- Bouillon, S., Fichefet, T., Legat, V., & Madec, G. (2013). The elastic-viscous-plastic method revisited. *Ocean Modelling*, 71, 2–12. <https://doi.org/10.1016/j.ocemod.2013.05.013>
- Danilov, S., Koldunov, N., Sidorenko, D., Scholz, P., & Wang, Q. (2021). Revisiting the implementation of EVP sea ice dynamics files. <https://doi.org/10.5281/zenodo.4667735>
- Danilov, S., Sidorenko, D., Wang, Q., & Jung, T. (2017). The Finite-volume Sea ice–Ocean Model (FESOM2). *Geoscientific Model Development*, 10, 765–789. <https://doi.org/10.5194/gmd-10-765-2017>
- Danilov, S., Wang, Q., Timmermann, R., Iakovlev, N., Sidorenko, D., Kimmritz, M., et al. (2015). Finite-element sea ice model (FESIM), version 2. *Geoscientific Model Development*, 8(6), 1747–1761. <https://doi.org/10.5194/gmd-8-1747-2015>
- Harris, C. R., Millman, K. J., van der Walt, S. J., Gommers, R., Virtanen, P., Cournapeau, D., et al. (2020). Array programming with NumPy. *Nature*, 585(7825), 357–362. <https://doi.org/10.1038/s41586-020-2649-2>
- Hibler, W. D., III (1979). A dynamic thermodynamic sea ice model. *Journal of Physical Oceanography*, 9, 815–846. [https://doi.org/10.1175/1520-0485\(1979\)009<0815:adtsim>2.0.co;2](https://doi.org/10.1175/1520-0485(1979)009<0815:adtsim>2.0.co;2)
- Hoyer, S., & Hamman, J. (2017). xarray: N-D labeled arrays and datasets in Python. *Journal of Open Research Software*, 5(1). <https://doi.org/10.5334/jors.148>
- Hunke, E. C. (2001). Viscous-plastic sea ice dynamics with the EVP model: Linearization issues. *Journal of Computational Physics*, 170, 18–38. <https://doi.org/10.1006/jcph.2001.6710>
- Hunke, E. C., & Dukowicz, J. K. (1997). An elastic-viscous-plastic model for sea ice dynamics. *Journal of Physical Oceanography*, 27, 1849–1867. [https://doi.org/10.1175/1520-0485\(1997\)027<1849:aevpmlf>2.0.co;2](https://doi.org/10.1175/1520-0485(1997)027<1849:aevpmlf>2.0.co;2)
- Hunter, J. D. (2007). Matplotlib: A 2d graphics environment. *Computing in Science & Engineering*, 9(3), 90–95. <https://doi.org/10.1109/MCSE.2007.55>

- Kimmritz, M., Danilov, S., & Losch, M. (2015). On the convergence of the modified elastic-viscous-plastic method for solving the sea ice momentum equation. *Journal of Computational Physics*, 296, 90–100. <https://doi.org/10.1016/j.jcp.2015.04.051>
- Kimmritz, M., Danilov, S., & Losch, M. (2016). The adaptive EVP method for solving the sea ice momentum equation. *Ocean Modelling*, 101, 59–67. <https://doi.org/10.1016/j.ocemod.2016.03.004>
- Kimmritz, M., Losch, M., & Danilov, S. (2017). A comparison of viscous-plastic sea ice solvers with and without replacement pressure. *Ocean Modelling*, 115, 59–69. <https://doi.org/10.1016/j.ocemod.2017.05.006>
- Koldunov, N. V., Aizinger, V., Rakowsky, N., Scholz, P., Sidorenko, D., Danilov, S., & Jung, T. (2019). Scalability and some optimization of the Finite-volumeE Sea ice–Ocean Model, version 2.0 (FESOM2). *Geoscientific Model Development*, 12, 3991–4012. <https://doi.org/10.5194/gmd-12-3991-2019>
- Koldunov, N. V., Danilov, S., Sidorenko, D., Hutter, N., Losch, M., Goessling, H., et al. (2019). Fast EVP solutions in a high-resolution sea ice model. *Journal of Advances in Modeling Earth Systems*, 11. <https://doi.org/10.1029/2018ms001485>
- Lemieux, J.-F., Knoll, D., Tremblay, B., Holland, D., & Losch, M. (2012). A comparison of the Jacobian-free Newton-Krylov method and the EVP model for solving the sea ice momentum equation with a viscous-plastic formulation: A serial algorithm study. *Journal of Computational Physics*, 231(17), 5926–5944. <https://doi.org/10.1016/j.jcp.2012.05.024>
- Mehlmann, C., Danilov, S., Losch, M., Lemieux, J.-F., Hutter, N., Richter, T., et al. (2021). *Simulating linear kinematic features in viscous-plastic sea ice models on quadrilateral and triangular grids*. Retrieved from <http://arxiv.org/abs/2103.04431>
- Met Office. (2010–2015). *Cartopy: A cartographic python library with a matplotlib interface*.
- Steele, M., Morley, R., & Ermold, W. (2001). PHC: A global ocean hydrography with a high-quality Arctic Ocean. *Journal of Climate*, 14(9), 2079–2087. [https://doi.org/10.1175/1520-0442\(2001\)014<2079:pagoHW>2.0.CO;2](https://doi.org/10.1175/1520-0442(2001)014<2079:pagoHW>2.0.CO;2)
- Tsujino, H. E. A. (2018). JRA-55 based surface dataset for driving ocean–sea-ice models (JRA55-do). *Ocean Modelling*, 130, 79–139. <https://doi.org/10.1016/j.ocemod.2018.07.002>
- Wang, Q., Danilov, S., Jung, T., Kaleschke, L., & Wernecke, A. (2016). Sea ice leads in the Arctic Ocean: Model assessment, interannual variability and trends. *Geophysical Research Letters*, 43(13), 7019–7027. <https://doi.org/10.1002/2016gl068696>